Novel SOLPS-ITER Simulations of X-point target and Snowflake Divertors

C Cowley[1,3], A Q Kuang[2], D Moulton[3], J D Lore[4], J Canik[4], M Umansky[5], M Wigram[2], S Ballinger[2] and B Lipschultz[1]

[1] York Plasma Institute, University of York, Heslington, York, YO10 5DQ, UK

[2] MIT Plasma Science and Fusion Center, 167 Albany St, Cambridge, MA 02139, United States

[3] UKAEA-CCFE, Culham Science Centre, Abingdon, OX14 3DB, UK

[4] Oak Ridge National Laboratory, 5200, 1 Bethel Valley Rd, Oak Ridge, TN 37830, United States

[5] Lawrence Livermore National Laboratory, 7000 East Ave., Livermore CA 94550

E-mail: `czlc500@york.ac.uk`

Abstract.

The design and understanding of alternative divertor configurations may be crucial for achieving acceptable steady-state heat and particle material loads for magnetic confinement fusion reactors. Multiple x-point alternative divertor geometries such as Snowflakes and X-point targets have great potential in reducing power loads, but have not yet been simulated widely in codes with kinetic neutrals. This paper discusses recent changes made to the SOLPS-ITER code to allow for the simulation of X-point target and low-field side snowflake divertor geometries. Snowflake simulations using this method are presented, in addition to the first SOLPS-ITER simulation of the X-point target. Analysis of these results show reasonable consistency with the simple two point model, supporting the validity of the methodology implemented for these novel simulations.

1. Introduction

Maintaining manageable heat and particle loads on materials presents a significant challenge to overcome for high power magnetic confinement fusion reactors. For reactor-like machines such as ITER and SPARC [1], empirical scalings predict deposited target heat loads in excess of 25MWm^{-2} [2, 3]; significantly higher than the 15 MWm^{-2} steady-state surface heat load limit on tungsten monoblock tiles [4]. Additionally, the high loads of energetic particles in these machines can lead to erosion rates of more than 15nm s^{-1} [2] on tungsten tiles, limiting the effective lifetime of these tiles and requiring more frequent, costly replacement of the divertor components. As a consequence, methods of reducing heat and particle loads in the divertor will be important for operating future devices; methods such as injecting radiating impurities and operating with alternative divertors.

Alternative divertors are divertors which leverage novel magnetic or geometric features differing from the 'standard' divertor; features which are predicted to benefit divertor exhaust in some way. One such alternative divertor is the Snowflake, which implements additional nulls near primary X-point, creating a higher order X-point, which has been shown to significantly increase divertor connection lengths [5] and may enhance cross-field transport through churning modes [6]. The X-point target (XPT) is another alternative divertor, which has a secondary X-point near the divertor targets [7]. The low poloidal field near this secondary X-point can lead to longer connection lengths, and there can be significant power sharing between the multiple outer divertor targets - depending on the X-point separation and strength of cross-field transport [8, 9]. Furthermore, the secondary X-point can be located at higher major radius than the primary, creating a magnetic flux expansion and lowering heat flux densities at the targets (similar to the Super-X divertor configuration [10]). Finally, the low poloidal field and local minimum in total field created by the secondary X-point could aid in detachment control [11, 12].

Despite the potential of Snowflake and XPT divertors, neither geometry has been widely simulated in codes with kinetic neutrals, particularly in the simulation code SOLPS-ITER [13]. In fact, snowflakes have only been simulated once before in SOLPS-ITER [14], and

XPTs have never been simulated previously using the code due to the rigidity of the physics modules and grid generators [15]. The benefits of using SOLPS-ITER include the complex kinetic treatment of neutrals through its coupling to the EIRENE Monte-Carlo solver, the ability to activate drifts and currents, and the extensive history and benchmarking of the code [15]. In this work we propose a new generalised method for simulating both X-point target and low-field side snowflake divertors within SOLPS-ITER, which may allow more widespread simulation of these alternative geometries; furthering the understanding of such divertors. Compared to the work performed in [14], the modifications to SOLPS-ITER have been generalized and do not affect the ability to run standard configurations.

2. Methodology

When running a SOLPS-ITER simulation of a new geometry, it is first necessary to generate relevant input files. This is typically done using a combination of the DivGeo software for basic input specification, the standard grid builder CARRE [16], and other preprocessing routines such as Unip, which generates template input files based on the grid geometry as set up by the DivGeo graphical interface (further information on the submodules can be found in the SOLPS-ITER manual). After generating the relevant input files, the physics simulations can be run, which for SOLPS-ITER is typically a coupled simulation of the fluid solver B2.5 and the kinetic Monte Carlo code EIRENE [13].

However, the current version SOLPS-ITER only works for an expected list of geometries, including single null divertors, double null divertors, slab geometries, and stellarator islands. For more unconventional grids such as the XPT, there are two main issues that prevent using this standard workflow. First, the physics modules of SOLPS-ITER (i.e., the fluid solver B2.5 and the kinetic transport code EIRENE) expect a double null geometry if a grid is given that contains two X-points. The second issue is that the grid builder CARRE is unable to build grids using equilibria with two X-points between the midplane and the divertor targets.

Consequently, to run a SOLPS-ITER simulation of a snowflake or XPT requires solutions to these two issues. Solutions to these challenges have been developed throughout this work and will be presented in the following section.

2.1. Modifying SOLPS-ITER Source

The first challenge to be solved before XPT or snowflakes can be simulated in SOLPS-ITER is the fact that the fundamental physics modules are not expecting such geometries. Instead, when two X-points are detected in the geometry, SOLPS-ITER assumes the grid is a double null. These assumptions are present because the B2.5 plasma grid must be rectangular when mapped into poloidal and radial index coordinates. In a slab geometry this mapping is simple, as the cell neighbors in poloidal and radial index space are physically adjacent when mapped to real coordinates. However, the introduction of X-points or more than two

targets introduces 'cuts', where the poloidal neighbor of a cell is not the cell that is adjacent in physical space. To prepare the geometry correctly, SOLPS-ITER assumes a certain order of X-point and target cuts. If two disconnected X-points are detected, the code assumes the ordering is that of a disconnected double null (DDN), which is shown in Figure 1.

Figure 2 shows the geometry of a lower XPT and its rectangular mapping, which is similar to a snowflake with the secondary X-point on the low-field side. From Figures 1 and 2, one can see that the DDN and XPT geometries are similar, with three radial regions, four cuts due to X-points, and one cut due to intermediate targets. However, the figure also shows that the ordering of these cuts is subtly but crucially different. For example, in the DDN case the target cut is the 3rd cut to be encountered poloidally, whereas in the XPT case the intermediate targets comprise the 4th poloidal cut. Moreover, if we label the primary X-point as 1, and the secondary as 2, then in order of increasing in poloidal index the DDN encounters 1,2,2,1; contrarily, the XPT encounters 1,1,2,2.

Because the ordering of XPT cuts are different from what SOLPS-ITER expects, a standard run of the code will fail if an X-point target or Snowflake grid is provided. To overcome this, several B2.5 preprocessing routines, and B2.5-EIRENE interfacing routines were edited to detect whether a grid has a DDN or an XPT (equivalently a low-field side Snowflake) ordering of primary and secondary X-point cuts. If a DDN is detected, the code will run in its unedited form, expecting the cut order shown in Figure 1. If an XPT is detected, however, new code has been written to unpack grid data according to an ordering of cuts shown in Figure 2. With this modified code, XPTs/low-field side snowflakes can be simulated without taking away from any previous SOLPS-ITER functionality. The code modifications have not yet been implemented to allow for a high-field side snowflake, though this could be achieved in much the same way.

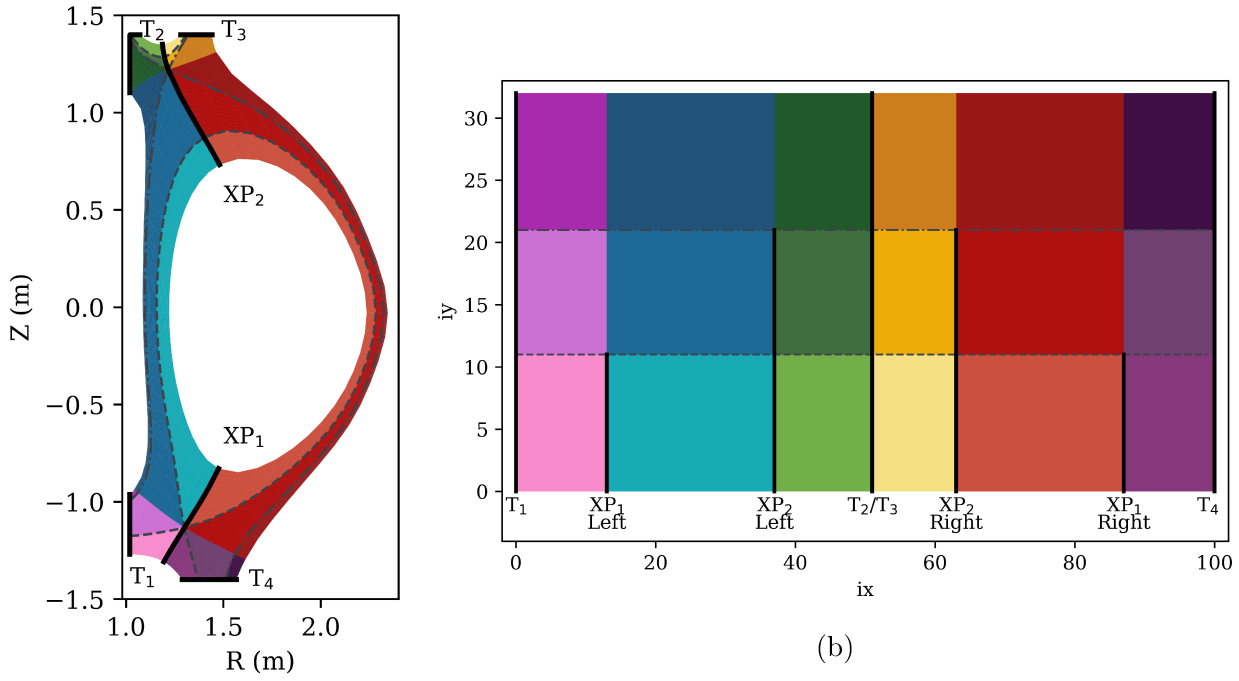

(a) (b)

Figure 1: The patch diagrams of a disconnected double null divertor mapped in a) physical coordinates and b) poloidal and radial index coordinates.

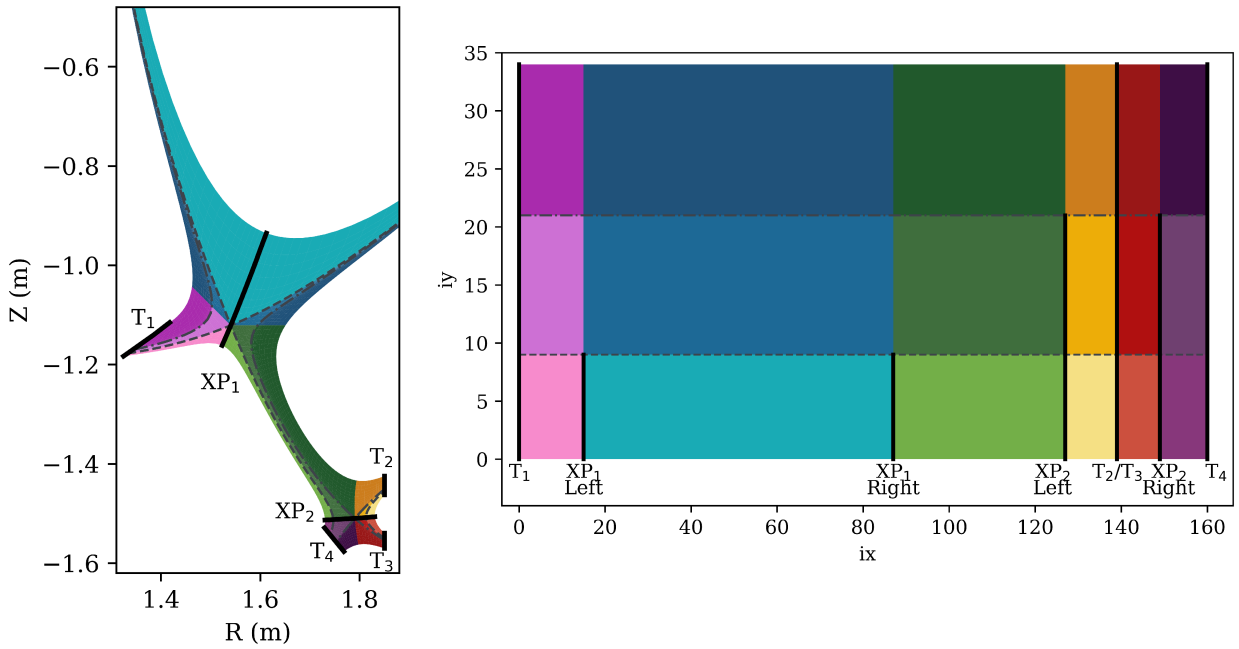

Figure 2: The patch diagrams of a lower X-point target divertor mapped in a) physical coordinates and b) poloidal and radial index coordinates.

2.2. Input File Generation

The second issue to overcome in simulating XPTs or snowflakes in SOLPS-ITER is the fact that relevant input files cannot be generated through the normal workflow of DivGeo, CARRE, and Unip. This is due to the fact that DivGeo and CARRE are not configured to deal with XPT or Snowflake equilibria. As such, a custom workflow was developed to prepare the required input files for a SOLPS-ITER run without the use of CARRE. This workflow consists of three unique steps, followed by a continuation of the regular SOLPS-ITER workflow.

The first step in the custom XPT simulation workflow is similar to that of a regular workflow, in that it revolves around generating a basic input structure with the graphical user interface DivGeo. Plasma facing components (PFCs) are loaded into DivGeo and adjusted manually if necessary, as shown in Figure 3a. The plasma species, wall material, and recycling coefficients are specified. A disconnected double null equilibrium should be loaded into DivGeo as a placeholder, which allows the basic .trg, .str and .dgo files to be generated. The preprocessing routine Unip should then be run on these files to produce a template EIRENE input file input.dat. This file will have incorrect plasma grid information, but will contain the correct specification of material boundaries. Using DivGeo in this way is similar to how linear device input files are generated in SOLPS-ITER [17].

In addition to creating an input.dat template, DivGeo should also be used to export individual surface structures used for later steps in this workflow. In particular, the inner and outer targets should be exported, along with the four 'contour' surfaces, which join the edges of each of the four targets. These surfaces are necessary for generating the EIRENE triangles in later steps, and an example of these surfaces is shown in Figure 3a.

The second step of this process is generating the XPT grid mesh from an equilibrium. To do this, we have used INGRID [18], a grid generator than can use snowflake and X-point target equilibria, among others. Here the radial plasma boundaries are manually adjusted to allow a suitable plasma simulation domain, but are still within rough limits of PFCs. Poloidal boundaries are determined by the target locations, which can be fed into INGRID using the exported target data from DivGeo. Parameters such as grid distortion and cell spacing can be manually modified in INGRID until a grid of the desired resolution and orthogonality is achieved. The patch data from a INGRID run can be seen in Figure 3b.

INGRID will output a gridue file, which contains magnetic field and grid vertex data. This data, however, must be read and converted to .geo files, which is done through python scripts. After the grid data is generated and converted to the appropriate format, the third step is to write key SOLPS-ITER input files. Of course, in the first DivGeo step many of these input files have been generated, but are not written correctly for an XPT. Thus, python routines have been written to edit templates of the following files and fill them with appropriate grid data: input.dat, b2ag.dat, b2ah.dat, b2.boundary.parameters, b2.neutrals.parameters. Finally, python routines have also been written to create tria.in file from the contours exported from DivGeo. After this third step, all geometry-dependent

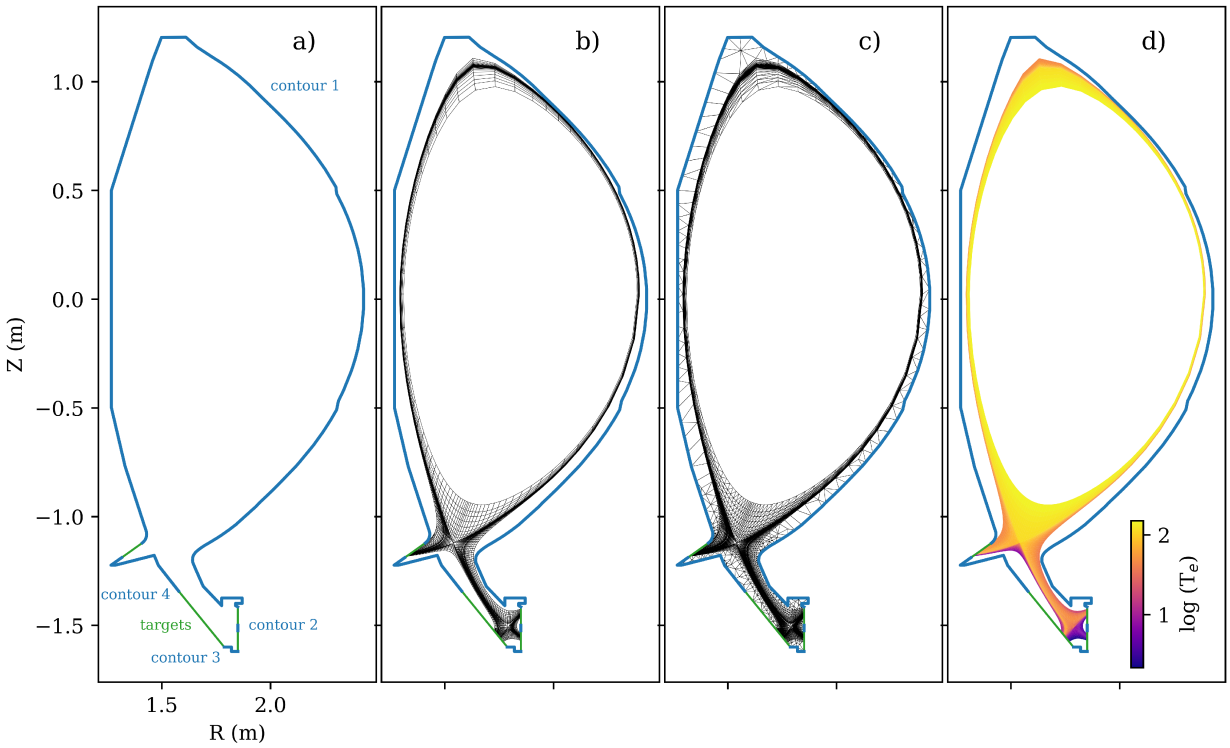

Figure 3: a) The target structures and contours exported by DivGeo. b) The grid of an XPT equilibrium generated by INGRID. c) The EIRENE triangles for an XPT grid generated with using the standard TRIA routines and contours exported by DivGeo. d) The electron temperature profile of a converged SOLPS-ITER simulation of a XPT equilibrium.

input files should be generated, and the remaining input files such as b2ar.dat can be written manually according to a user's preference.

2.3. Submitting a Simulation

After the basic input files have been generated, the regular SOLPS-ITER preprocessing routines can be run. On the fluid side this includes b2ag, the geometry preparation routine, b2ah which prepares plasma boundary conditions, b2ai which prepares the initial plasma state, and b2ar which prepares the rates. For EIRENE, the routine TriaGeom must be run to create the triangles which will be used as a domain for the kinetic Monte-Carlo transport code. The successful output of a TriaGeom run for the SPARC XPT can be seen in Figure 3c.

Finally, when all preprocessing routines are finished, a b2mn.dat file can be manually written, which specifies basic simulation run parameters. Then the simulation should be run until convergence is achieved. This has been achieved for the first time for an XPT grid in SOLPS-ITER, with an example shown in Figure 3d. The corresponding results are discussed in the following section.

3. X-point Target Results

For this study two test simulations were carried out to verify the modified code and workflow. These simulations were of a SPARC lower single null (SN), and a SPARC lower XPT equilibrium where the two separatrixes are 0.4mm apart mapped to the outer midplane. The XPT grid files were generated using the novel workflow in Section 2, whereas the SN input files were generated using the standard CARRE workflow as a benchmark for comparison. PFC contours for both simulations are based upon those of SPARC, but are modified to allow a wider simulation domain. When the relevant input files were obtained, both simulations were run with the same coupled SOLPS-ITER routines. Both grids were roughly matched in terms of radial boundaries; the single null extending from -7.4mm to +1.7mm from the separatrix at the outer midplane, and the XPT extending from -7.8mm to +2.0mm.

The SN and XPT simulations were pure deuterium simulations without drifts. The same input power of 200 kW and approximately the same outer midplane density of 1.15E19 m^{-3} were used for both simulations. Note that these values are not representative of SPARC, but have been used to access a regime of modest heat and particle flux (where extensive validation of SOLPS-ITER has been performed) without the need for impurities. The transport coefficients were also held constant for both runs, to achieve a $\approx$ 0.4 mm heat flux fall off width at the X-point and a $\approx$ 4mm density fall off width at the outer midplane. Crucially, because no impurities are used, and because both grids have similar total flux expansions, the SN and XPT simulations should have similar heat flux density profiles. Thus, the agreement of these simulations can serve as an effective benchmark for the new code changes and workflow.

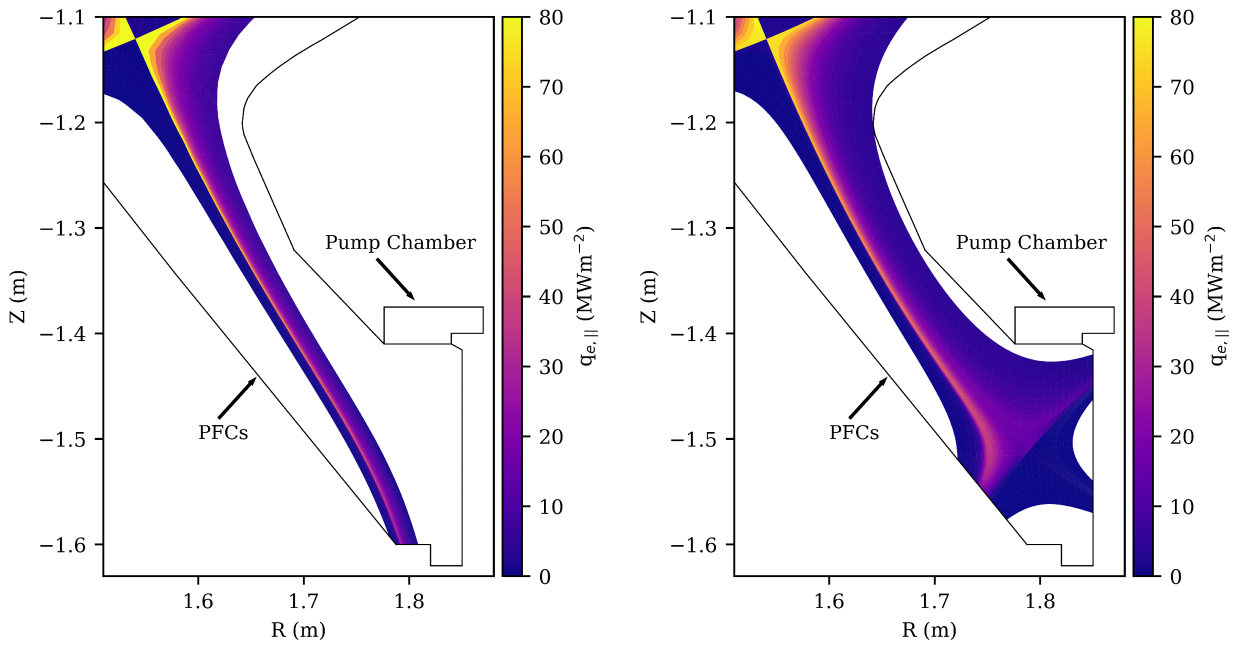

(a) (b)

Figure 4: The 2D electron heat flux density profile of a a) SPARC SN and b) SPARC XPT SOLPS-ITER simulation. PFCs are shown in black.

The 2D parallel electron heat flux density profiles of the SN and XPT simulations are shown in Figures 4a and 4b respectively. From these figures, it is clear to see good overall qualitative agreement between the two grids, both in profile shape further upstream and the maximum and minimum heat flux values throughout the divertor. Furthermore, the radial profiles of the electron heat flux density at the divertor entrance can be seen in Figures 5a and 5b, and also show good quantitative and qualitative agreement. In particular, both profiles show a peak heat flux density of 80 MWm^{-2}, and a fall-off width of $\approx$ 0.4mm.

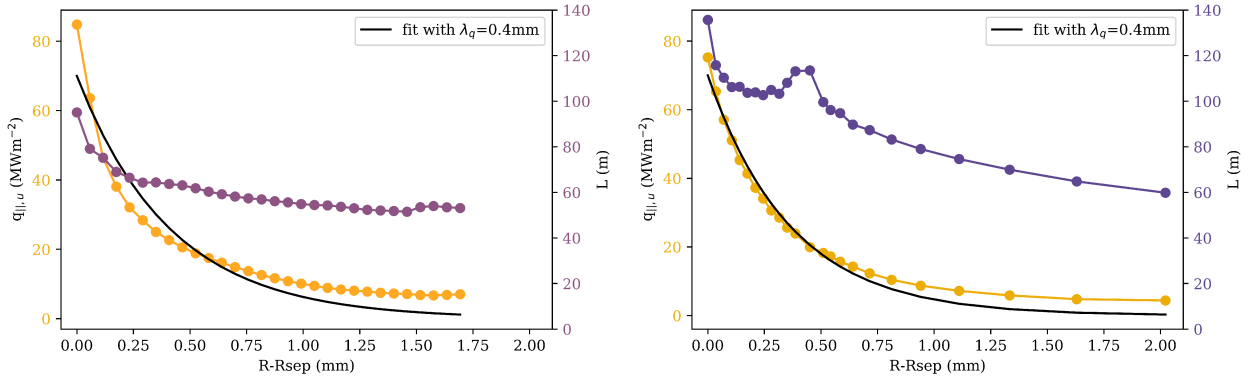

(a) (b)

Figure 5: The upstream electron conducted heat flux density profiles as a function of radial distance from the separatrix (mapped to the outer midplane) for a) a SPARC single null divertor and b) a SPARC XPT divertor. The data corresponding to the right axes in purple shows the radial connection length profile of each grid.

Similarly, the upstream electron density and temperature profiles are plotted and shown in Figures 6a and 6b. These figures show similar yet not exactly identical profiles, with a maximum deviation in temperature and density of 10-15%. This may be attributed to the difference in connection length over the SOL, which can be seen in Figures 5a and 5b.

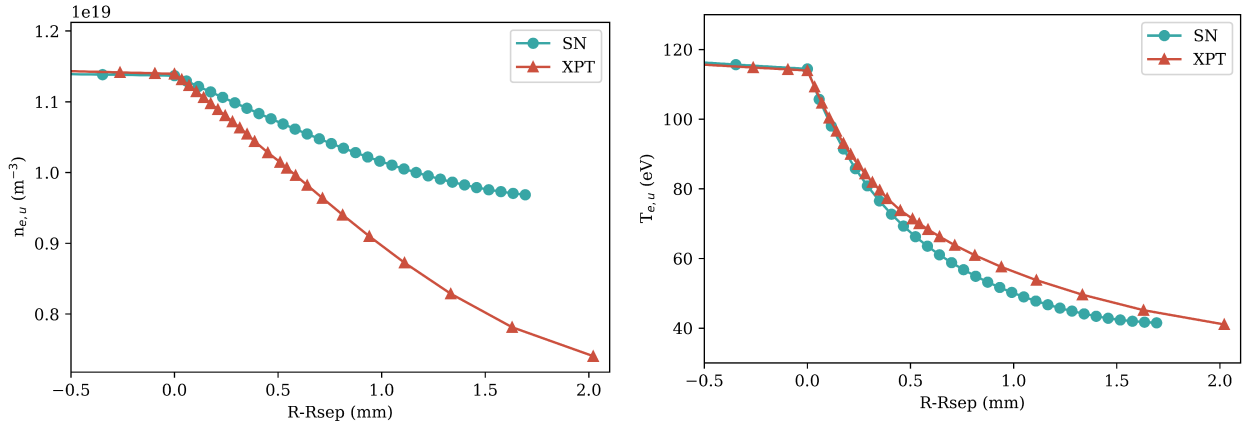

(a) (b)

Figure 6: The upstream a) electron density and b) electron temperature profiles as a function of radial distance from the separatrix (mapped to the outer midplane) for a SPARC single null and XPT divertor.

Given that the upstream profiles of the two grids are similar, and that there are no strong heat dissipation mechanisms such as impurities, then the target pressure and parallel heat flux density profiles in the two cases should be similar. Indeed, the target electron heat flux

density and static pressure are plotted in Figures 7a and 7b, and show a similar qualitative profile between the single null and XPT grids. Moreover, when the target profiles for the two primary targets for the X-point target are overlaid, they form one relatively continuous profile apart from at the secondary X-point at ≈ 0.4mm from the primary separatrix. This tends to support the idea that these physics simulations are running with no issues, and that the baseline grid is mapped correctly.

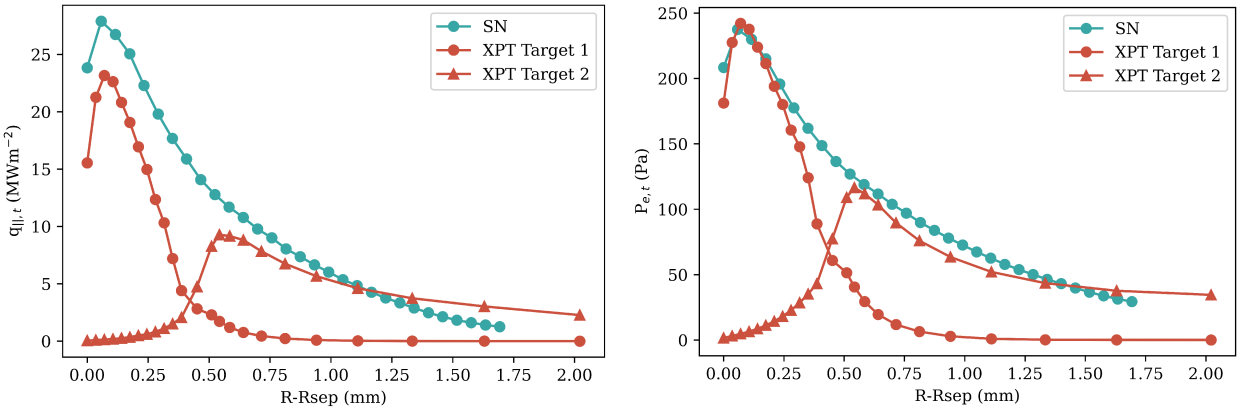

(a) (b)

Figure 7: The target electron a) heat flux density and b) static pressure profiles as a function of radial distance from the separatrix (mapped to the outer midplane) for a SPARC single null and XPT divertor.

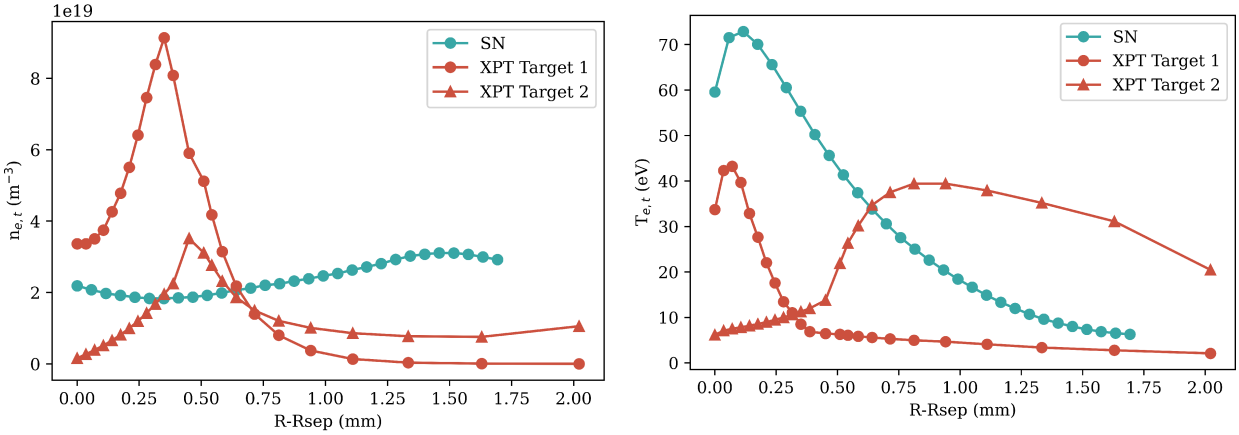

(a) (b)

Figure 8: The target electron a) density and b) temperature profiles as a function of radial distance from the separatrix (mapped to the outer midplane) for a SPARC single null and XPT divertor.

Finally, the target electron density and temperature profiles for both simulations are

plotted in Figures 8a and 8b. Unlike the heat flux and pressure profiles, these profiles differ significantly between the two grids. However, this is not unexpected given that ultimately the grids are not identical, and in fact the connection length profiles vary between the two. What is crucial to determine, therefore, is whether these differences in target parameters can be explained by physics analysis. Using simple arguments of the two point model, the target temperature should vary [19]:

$$T_u^{7/2} - T_t^{7/2} = q_{||,u} L \kappa_1 \tag{1}$$

Where $L_{||}$ is the connection length and κ_1 is the Spitzer conductivity divided by $T^{5/2}$, which is typically taken approximated as a constant simple two point model analysis. Consequently, given a constant κ_1 and assuming the heat flux density does not change significantly over the divertor volume, the difference in upstream and downstream temperatures to the power 7/2 should vary with $q_{||,u} L_{||}$. The profiles of connection length, the product of connection length and heat flux density, and the difference in upstream and downstream temperatures to the power 7/2 are plotted in Figure 9. Indeed, this figure shows the XPT simulation temperature profiles are in very good agreement with simple two point model physics. There is small deviation from the trend at R-R$_{sep}$ = 0.25mm, but this can be attributed to flux limited heat conduction and increased heat flux losses near the secondary separatrix.

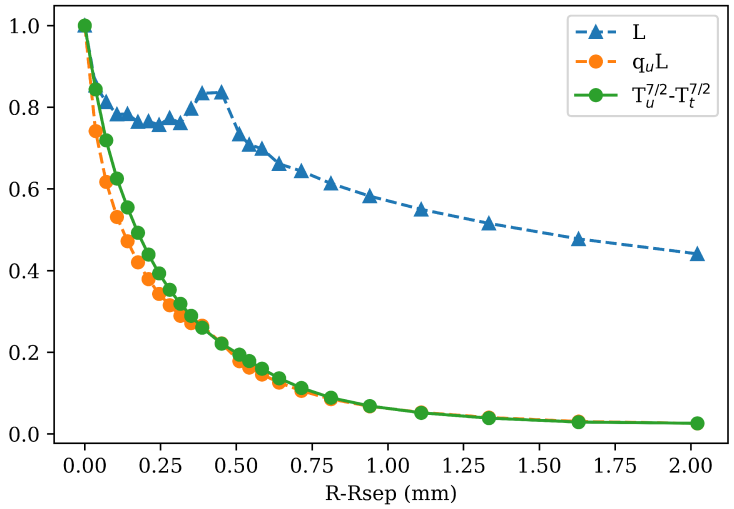

Figure 9: The profiles of connection length, the product of connection length and upstream electron heat flux density, and the difference in upstream target electron temperatures to the power 2/7, normalised to the values at the separatrix for a SPARC XPT simulation.

4. Snowflake Results

Simulations of a snowflake divertor have also been performed as part of the validation of this novel workflow. The equilibrium used is shown in Figure 10a and is similar to that of TCV,

though the PFCs are unique to this study. An input power and core density of 20 KW and 1.1×10^{19} m^{-3} were used, and the electron temperature profile of the converged solution is shown in Figure 10b. The profiles from this Figure are well behaved, and in general this configuration is not greatly effected by the presence of the secondary x-point. This is not unexpected, since the two x-points have a large poloidal separation, and this equilibrium was simply chosen for demonstration purposes.

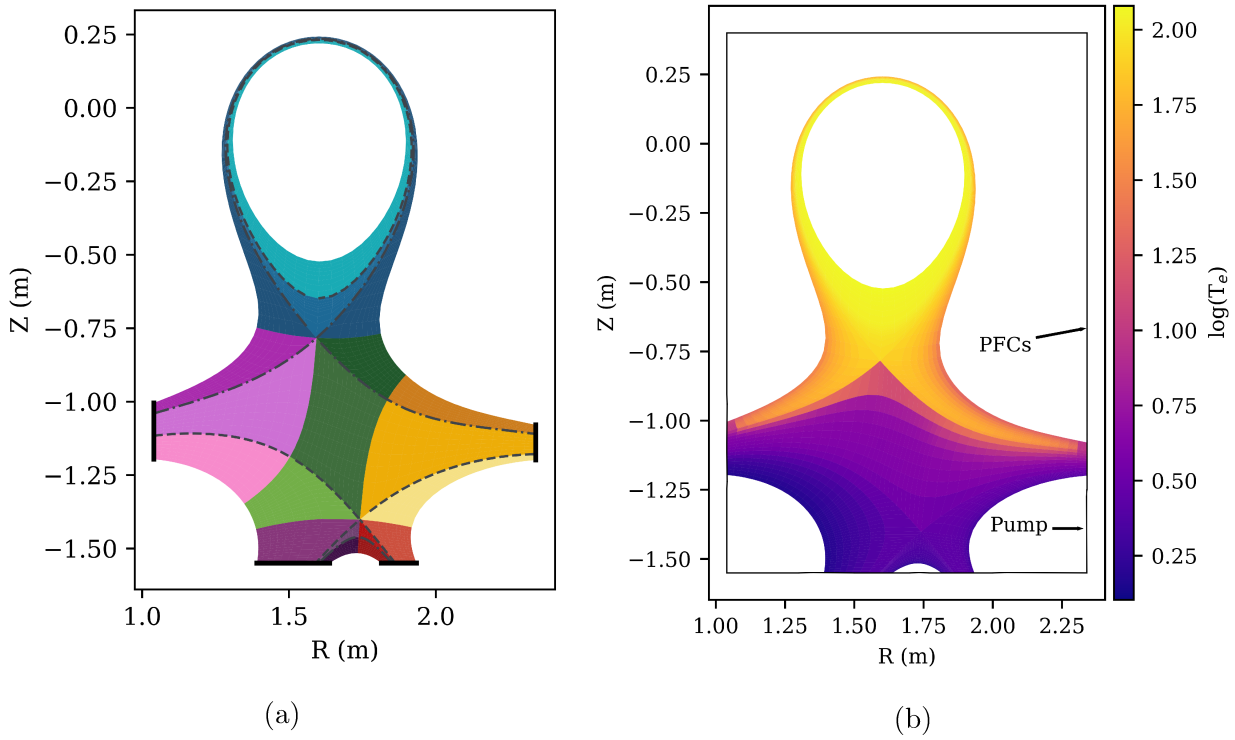

Figure 10: a) A patch diagram of a low-field side snowflake divertor. b) A logarithmic 2d electron temperature map of a converged SOLPS-ITER simulation of the equilibrium in a).

5. Conclusions

Throughout this work, a new way of simulating X-point target and low-field side snowflake divertors in SOLPS-ITER is presented. The SOLPS-ITER source has been edited to accept multiple X-point alternative divertors, whilst still maintaining functionality for standard double null divertors. INGRID, an interactive python grid generator has been used to generate the grid data, which is then converted into SOLPS-ITER ready input files using custom python routines. Results and analysis from SOLPS-ITER simulation of low power SPARC-like single null, SPARC-like X-point target, and TCV-like snowflake equilibria have been presented. The similarities between the two SPARC simulations, coupled with the consistency of simple two point model analysis on the XPT grid supports the validity of the results presented.

6. Acknowledgments

This work has been part-funded by the RCUK Energy Programme [grant number EP/T012250/1], and in part performed under the auspices of the U.S. DoE by LLNL under Contract DE-AC52-07NA27344.

This work has been carried out within the framework of the EUROfusion Consortium and has received funding from the Euratom research and training programme 2014-2018 and 2019-2020 under grant agreement No 633053. The views and opinions expressed herein do not necessarily reflect those of the European Commission.

The authors would like to acknowledge CFS for the SPARC equilibria and the TCV team for the snowflake equilibrium.

References

[1] Creely AJ, Greenwald MJ, Ballinger SB, Brunner D, Canik J, Doody J, et al. Overview of the SPARC tokamak. Journal of Plasma Physics. 2020;86(5):865860502.

[2] Loarte A, Lipschultz B, Kukushkin A, Matthews G, Stangeby P, Asakura N, et al. Power and particle control. Nuclear Fusion. 2007;47(6):S203.

[3] Kuang AQ, Ballinger S, Brunner D, Canik J, Creely AJ, Gray T, et al. Divertor heat flux challenge and mitigation in SPARC. Journal of Plasma Physics. 2020;86(5):865860505.

[4] Pitts R, Bonnin X, Escourbiac F, Frerichs H, Gunn J, Hirai T, et al. Physics basis for the first ITER tungsten divertor. Nuclear Materials and Energy. 2019;20:100696.

[5] Ryutov D. Geometrical properties of a "snowflake" divertor. Physics of Plasmas. 2007;14(6):064502.

[6] Ryutov D, Cohen R, Rognlien T, Umansky M. A snowflake divertor: a possible solution to the power exhaust problem for tokamaks. Plasma Physics and Controlled Fusion. 2012;54(12):124050.

[7] LaBombard B, Marmar E, Irby J, Terry J, Vieira R, Wallace G, et al. ADX: a high field, high power density, advanced divertor and RF tokamak. Nuclear Fusion. 2015;55(5):053020.

[8] Wigram MRK, LaBombard B, Umansky M, Kuang A, Golfinopoulos T, Terry J, et al. Performance assessment of long-legged tightly-baffled divertor geometries in the ARC reactor concept. Nuclear fusion. 2019;59(10):106052.

[9] Umansky M, Rensink M, Rognlien T, LaBombard B, Brunner D, Terry J, et al. Assessment of X-point target divertor configuration for power handling and detachment front control. Nuclear Materials and Energy. 2017;12:918-23.

[10] Valanju PM, Kotschenreuther M, Mahajan S, Canik J. Super-X divertors and high power density fusion devices. Physics of Plasmas. 2009;16(5):056110.

[11] Lipschultz B, Parra FI, Hutchinson IH. Sensitivity of detachment extent to magnetic configuration and external parameters. Nuclear Fusion. 2016;56(5):056007.

[12] Cowley C, Lipschultz B, Moulton D, Dudson B. Optimizing detachment control using the magnetic configuration of divertors. Nuclear Fusion. 2022;62(8):086046.

[13] Schneider R, et al. SOLPS 2-D edge calculation code. Contrib Plasma Phys. 2006;46:3-191.

[14] Pan O, Lunt T, Wischmeier M, Coster D, Stroth U, et al. SOLPS-ITER modeling with activated drifts for a snowflake divertor in ASDEX Upgrade. Plasma Physics and Controlled Fusion. 2020;62(4):045005.

[15] Wiesen S, Reiter D, Kotov V, Baelmans M, Dekeyser W, Kukushkin A, et al. The new SOLPS-ITER code package. Journal of nuclear materials. 2015;463:480-4.

[16] Marchand R, Dumberry M. CARRE: a quasi-orthogonal mesh generator for 2D edge plasma modelling. Computer Physics Communications. 1996;96(2):232-46.

[17] Sala M, Tonello E, Uccello A, Bonnin X, Ricci D, Dellasega D, et al. Simulations of Argon plasmas in the linear plasma device GyM with the SOLPS-ITER code. Plasma Physics and Controlled Fusion. 2020;62(5):055005.

[18] Garcia B, Umansky M, Watkins J, Guterl J, Izacard O. INGRID: an interactive grid generator for 2D edge plasma modeling. Computer Physics Communications. 2022;275:108316.

[19] Stangeby PC, et al. The plasma boundary of magnetic fusion devices. vol. 224. Institute of Physics Pub. Philadelphia, Pennsylvania; 2000.